JOC The Journal of Organic Chemistry

Article

pubs.acs.org/joc

# Understanding the Mechanism of the Lewis Acid Promoted [3 + 2] Cycloaddition of Propargylic Alcohol and α-Oxo Ketene Dithioacetals

Haiyan Yuan, Yiying Zheng, and Jingping Zhang*

Faculty of Chemistry, Northeast Normal University, Changchun 130024, Jilin, China

Supporting Information

**ABSTRACT:** The mechanism and origin of selectivities in $BF_3$·$Et_2O$-catalyzed intermolecular [3 + 2] cycloadditions of propargylic alcohol and α-oxo ketene dithioacetals have been studied using density functional theory. Several possible reaction pathways were evaluated on the basis of two possible binding modes between the carbonyl or hydroxyl oxygen of substrates and catalyst. The preferred mechanism initiates dehydroxylation of propargylic alcohol by Lewis acid $BF_3$ and generates active allenic carbocation species to provide the favorable electrophile. It then proceeds via four processes involving nucleophilic addition of $C^{\alpha}$ on α-oxo ketene dithioacetals to the C1 of active allenic carbocation intermediate, [1,4]-alkylthio shift, $H^{\alpha}$-elimination, and intramolecular cyclization. This reaction sequence is in contrast to the mechanism by a previously published study, that is, [1,4]-alkylthio migration occurs prior to the cyclization. Our calculated results suggested that electrostatic attraction and hydrogen-bonding interactions between substrates and catalyst play a vital role in the [3 + 2] cycloaddition.

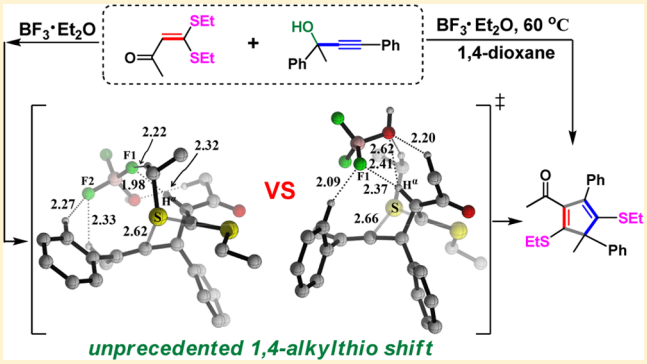


## INTRODUCTION

Functionalized five-membered carbocycles as structural motifs are often found in a large number of natural products and bioactive molecules.[1−3] The [3 + 2] cycloaddition reactions have attracted increasing interest in organic chemistry due to their wide application in the synthesis of various compounds with five-membered rings.[4,5] Among many impressive methods, transition-metal and phosphine-catalyzed [3 + 2] cycloaddition provide a powerful synthetic approach to obtain cyclopentadienes and cyclopentenes.[6,7] Despite the above significant achievements, the design and development of novel catalyst-mediated processes, beginning with easily available materials to afford densely functionalized cyclopentadienes, are still of great value. Very recently, the Bi group[8] reported a new class of fully substituted 2,5-dialkylthio cyclopentadienes using α-oxo ketene dithioacetals as the polarized alkene component instead of classic alkylthio displacement reactions[9] for the synthesis of carbocycles. They developed a novel strategy for the synthesis of cyclopentadienes by the $BF_3$·$Et_2O$-catalyzed regiospecific [3 + 2] cycloaddition of propargylic alcohols and α-oxo ketene dithioacetals (Scheme 1). Adequate understanding of the mechanistic details would certainly help exploit the latent potential of multicatalytic cascades. In the present study, we aim to shed light on the mechanism and the effective catalyst form of the $BF_3$·$Et_2O$ as well as the combinational sites between catalyst and substrates.

The mechanisms proposed by Bi et al. (red arrow mark) and us (blue arrow mark) are shown in Scheme 2. Four differences are found as follows. (1) The mechanism proposed by Bi includes $BF_3$·$Et_2O$-catalyzed dehydroxylation, nucelophilic addition of $C^{\alpha}$ of α-oxo ketene dithioacetals (**Re1**) on C3 of propargylic alcohols (**Re2**), intramolecular cyclization, stepwise [1,4]-alkylthio shift, and $[BF_3$·$OH]^-$ assisted H-elimination. However, our mechanism proceeds via $BF_3$-catalyzed dehydroxylation of **Re2**, $BF_3$·OH-assisted nucelophilic addition, [1,4]-alkylthio shift, and concerted cyclization and $H^{\alpha}$ deprotonation. (2) They proposed that intramolecular cyclization occurs prior to [1,4]-alkylthio shift, whereas our computational results suggest that this is impossible because of the high activation energy barrier. (3) Our results indicated that the [1,4]-alkylthio shift is a concerted process, while theirs is a stepwise one. (4) $BF_3$·$Et_2O$ and $[BF_3$·$OH]^-$ only play an important role in the dehydroxylation and H-elimination steps in their case. Nevertheless, $BF_3$ and $[BF_3$·$OH]^-$ play a vital role in the whole reaction process and stabilize the structures of transition states via hydrogen-bonding and electrostatic interactions.

**Scheme 1. $BF_3$·$Et_2O$-Catalyzed [3 + 2] Cycloaddition of Propargylic Alcohols and α-Oxo Ketene Dithioacetals**

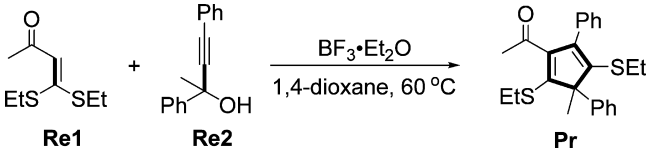


**Received:** December 13, 2015
**Published:** February 1, 2016





DOI: 10.1021/acs.joc.5b02826
J. Org. Chem. 2016, 81, 1989−1997

**Scheme 2. Mechanism Difference of $BF_3$-Catalyzed Propargylic Alcohols and α-Oxo Ketene Dithioacetals between Us (Blue Arrow Mark) and the Work of Bi et al. (Red Arrow Mark) Lies in the Reaction Sequence of the Intramolecular Cyclization and [1,4]-Alkylthio Shift**

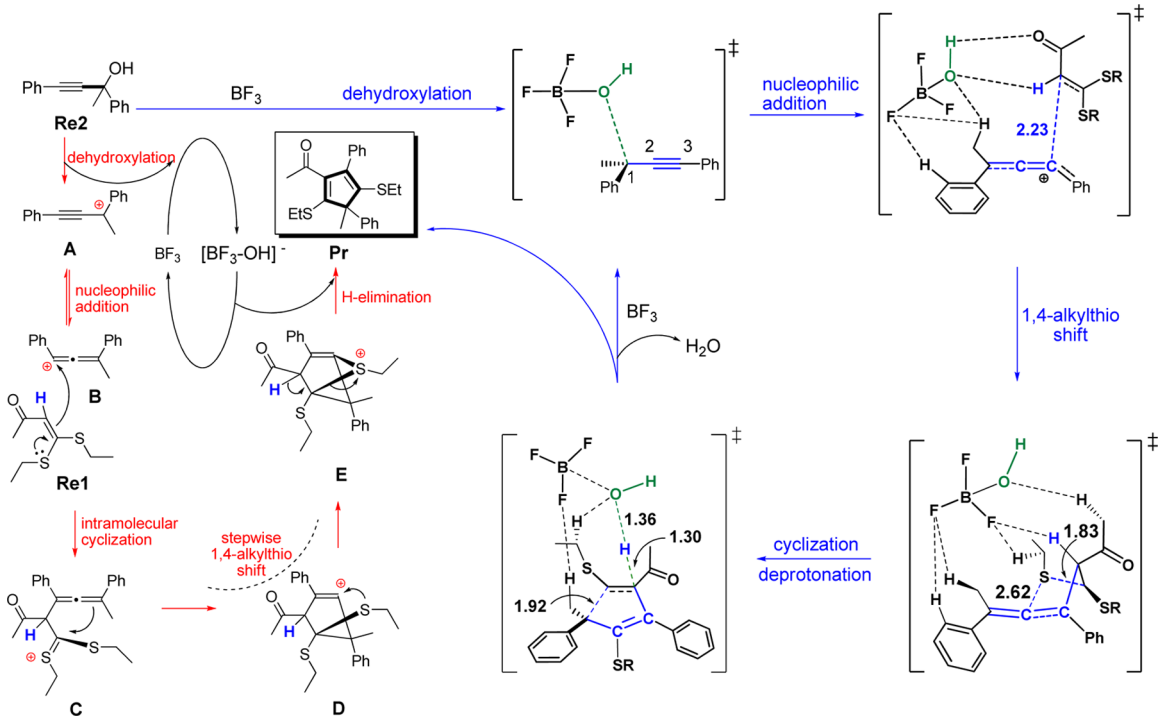


## COMPUTATIONAL METHODS

All calculations were performed using the Gaussian 09 suite of quantum chemical programs.[10] The hybrid density functional B3LYP (zero-point vibrational energies is scaled by 0.960) was used for geometry optimization with the 6-31+G** basis set for all atoms.[11] Frequency analysis was conducted at the same level of theory to characterize the stationary points and to obtain zero-point energy and thermal energy corrections at 333.15 K. The intrinsic reaction coordinate (IRC) calculations were carried out to confirm that all of the transition states were connected the corresponding reactants and products on the potential energy surface.[12] Moreover, it has been demonstrated that the B3LYP and M06-2X functionals can deal well with the C−H···F and C−H···O noncovalent interactions.[13,14] Thus, single-point energies were subsequently computed at the B3LYP-D[15] and M06-2X[13] levels using the 6-311+G** basis set in the solvent phase. D provides a better treatment of dispersion interactions, while M06-2X is better suited for handling kinetics, thermodynamics, and noncovalent interactions.[16,17] Solvent effects in 1,4-dioxane were evaluated using the Cramer−Truhlar continuum solvation model SMD.[18] The discussion employs the Gibbs free energies obtained at the M06-2X/6-311+G** level of theory. This method has been applied successfully to investigate the mechanisms of several catalytic organic reactions,[17a,19] which is generally considered to be more accurate for energetic.

Natural bond orbital (NBO) analysis[20] was carried out at the M06-2X/6-311+G** level to investigate the charge distribution and donor−acceptor interactions. To confirm the weak interactions, topological analysis of the electron densities within Bader's Atoms-in-Molecule (AIM) framework at the bond critical point explored using the Multiwfn program.[21] The optimized geometry structures are illustrated by CYLview.[22]

## RESULTS AND DISCUSSION

**3.1. Active Species for the Catalytic Reactions and Substrate Binding.** We explored first the effective catalyst form of Lewis acid $BF_3$·$Et_2O$ in the [3 + 2] cycloaddition of α-oxo ketene dithioacetals (**Re1**) and propargylic alcohols (**Re2**). The active $BF_3$ species dissociation from the $BF_3$·$Et_2O$ is endergonic with a relative free energy ($\Delta G$) of 10.5 kcal/mol (see eq 1). According to the mechanism of related reactions,[23] $BF_3$ could be easily formed from the reaction of precatalyst $BF_3$·$Et_2O$. Thus, our computational result implied that $BF_3$ acts as the real active catalyst to initiate the catalytic reaction. In addition, the vacant orbital on the boron atom of $BF_3$ can be well coordinated with the electron-rich O atom of the −OH group, namely, providing the electrophilic site.

$$BF_3{\cdot}Et_2O \rightarrow BF_3 + Et_2O \qquad \Delta G = 10.5 \text{ kcal/mol} \tag{1}$$

Before considering the various reaction pathways, we first evaluated the different modes of binding between the catalyst and the reactants. The coordination of the catalyst $BF_3$ to the hydroxyl oxygen of **Re2** (mode I) or the carbonyl oxygen of **Re1** (mode II) was considered. The results showed that coordination of mode I to give complex **I** is slightly less favored than that of mode II to form **II** by 0.9 kcal/mol, whereas the nucleophilic attack of $C^{\alpha}$ of **Re2** to allenic C3 of **Re1** for mode I is much more preferred by 39.3 kcal/mol (**TSI** vs **TSII**, Figure S1). Furthermore, the NBO charge calculation indicates that the charges on C3 and $C^{\alpha}$ in **I** or **II** are −0.435 and 0.112 or −0.530 and −0.122, respectively. Thus, we only discuss the coordination of mode I pathways herein. In addition, we also investigated the effect of interaction direction of hydroxyl of **Re2** and carbonyl of **Re1** on the activation Gibbs free energies.

**3.2. Mechanism of [3 + 2] Cycloaddition of Propargylic Alcohols and α-Oxo Ketene Dithioacetals.** Path A initiates from the complex **1** catalyzed by $BF_3$. The intermediate **I1** is formed via a dehydroxylation process and B−O bond formation transition state **TS1** with the activation free energy ($\Delta\Delta G^{\ddagger}$) of 18.4 kcal/mol (Figures 1 and 2). This



DOI: 10.1021/acs.joc.5b02826
J. Org. Chem. 2016, 81, 1989−1997

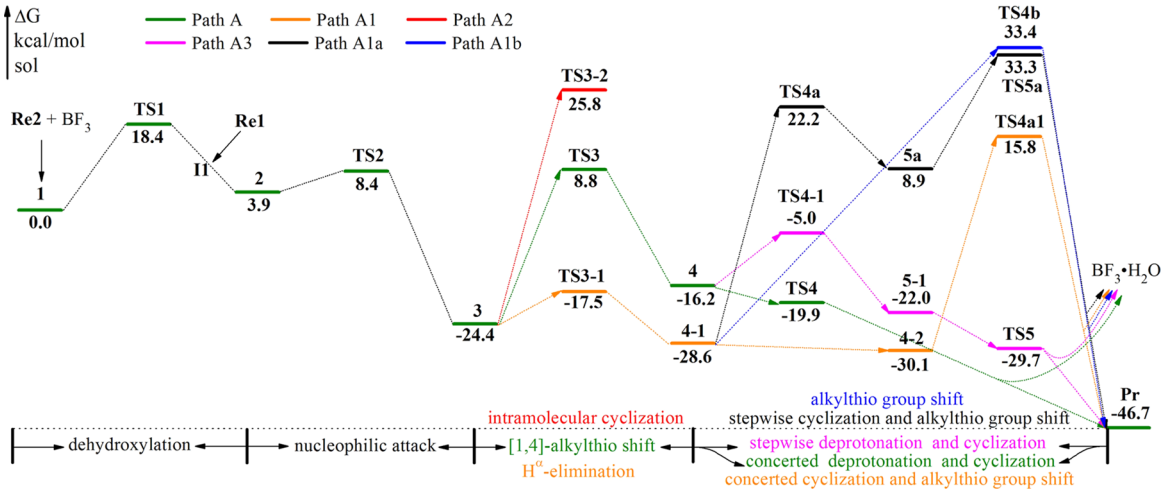


**Figure 1.** Free energy profiles of [3 + 2] cycloaddition of propargylic alcohols and $\alpha$-oxo ketene dithioacetals in the solvent phase.

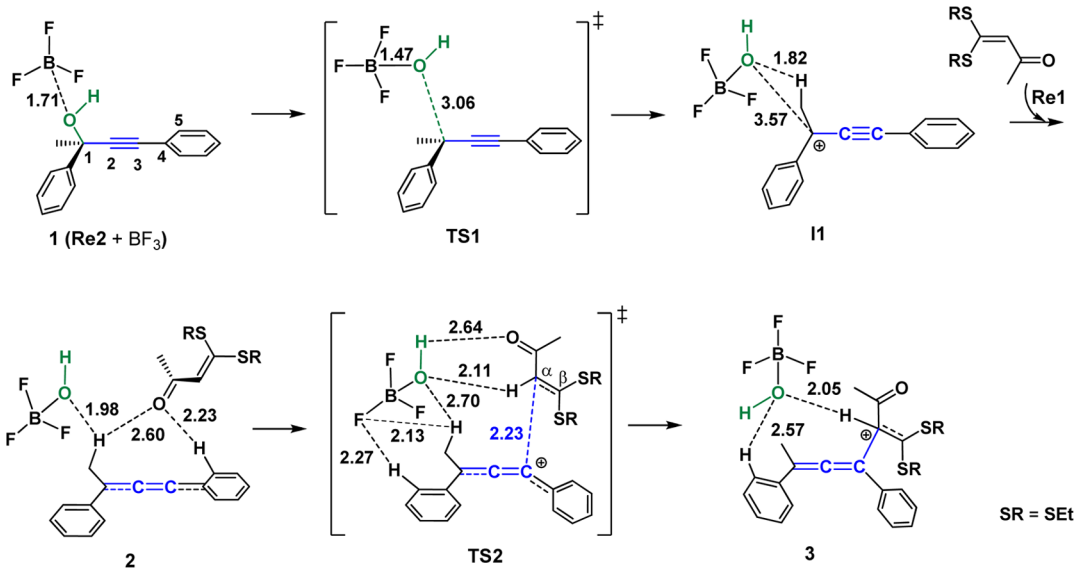


**Figure 2.** Geometry structures in dehydroxylation and nucleophilic attack processes. Distances are in Å.

process is facilitated by the strong electrostatic attraction between the B atom of $BF_3$ and the O atom of **Re2**. Then substrate **Re1** combines with intermediate **I1** and forms the intermediate **2**. This step is exothermic by 14.5 kcal/mol. Meanwhile, the carbocation transfers from the C1 to the allenic C3 due to the resonance stabilization and less sterically hindered of allenic carbocation intermediate **2**.[24] Furthermore, a careful inspection of structure for **TS1** suggests that its own electron-rich groups (−Ph and −Me) also contribute to the formation of the allenic carbocation C3 (Figure 2). The subsequent step is the nucleophilic attack of the $C^{\alpha}$ of **Re1** on the allenic C3 of **Re2** via transition state **TS2** with a free energy barrier of 8.4 kcal/mol, forming **3**. Quintuple hydrogen-bonding interactions (O−H···O, 2.64 Å; C−H···O, 2.11 and 2.70 Å; C−H···F, 2.13 and 2.27 Å) play an anchoring role by binding to the $C^{\alpha}$ and the C3 and stabilize the structure of **TS2**. From intermediate **3**, the reaction follows three alternative pathways (paths A, A1, and A2) differing in the sequence of [1,4]-alkylthio shift, $H^{\alpha}$-elimination, and cyclization (Figures 1 and 3). Path A is the $BF_3$-catalyzed alkylthio shift process. The alkylthio group shifts from $C^{\beta}$ to C2 via transition state **TS3** and generates intermediate **4**, requiring 33.2/8.8 kcal/mol of the $\Delta\Delta G^{\ddagger}/\Delta G$ value. In path A1, the $H^{\alpha}$ migrates from $C^{\alpha}$ to the −OH group of $BF_3$·OH via transition state **TS3-1** of 6.9 kcal/mol. Although path A1 is more advanced than path A by 26.6 kcal/mol, the latter one is still reasonable because the reactions need to be performed at 60 °C. This large energy difference is responsible for the [1,4]-alkylthio shift step forming a zwitterionic transition state/intermediate **TS3/4** with separated positive and negative charges, leading to **TS3/4** less stable than the neutral **TS3−1/4−1** in the 1,4-dioxane. The $\Delta\Delta G^{\ddagger}$ value of intramolecular cyclization transition state **TS3-2** in path A2 is 50.2 kcal/mol. Thus, cyclization occurs prior to [1,4]-alkylthio shift, $H^{\alpha}$-elimination is a kinetically inaccessible process, and path A2 can be excluded.

After intermediate **4**, two possible pathways (paths A and A3) were considered for the formation of the product **Pr** (Figures 1 and 4). In path A (**4** → **TS4** → **5**, Figure 4, green line), the C1−$C^{\beta}$ bond formation and $H^{\alpha}$ transfers from $C^{\alpha}$ to $[BF_3{\cdot}OH]^-$ simultaneously occur via a concerted transition state **TS4** to afford intermediate **5**, with the $\Delta\Delta G^{\ddagger}$ value of −3.7 kcal/mol. It is a barrier-free process. Finally, $BF_3$ and $H_2O$ are released to deliver the product **Pr**. Path A3 (**4** → **TS4−1** → **5−1** → **TS5**) is a stepwise process via deprotonation transition


DOI: 10.1021/acs.joc.5b02826
J. Org. Chem. 2016, 81, 1989−1997

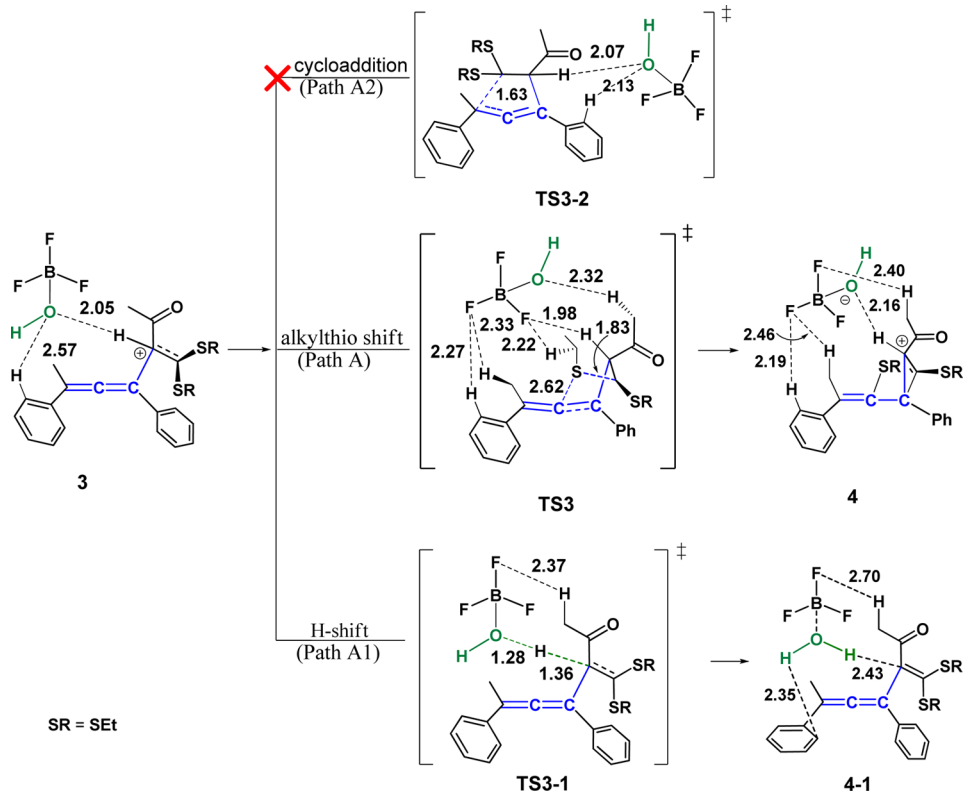


**Figure 3.** Comparison of the structures in [1,4]-alkylthio shift of path A, H-shift of path A1, and intramolecular cyclization of path A2. Distances are in angstroms.

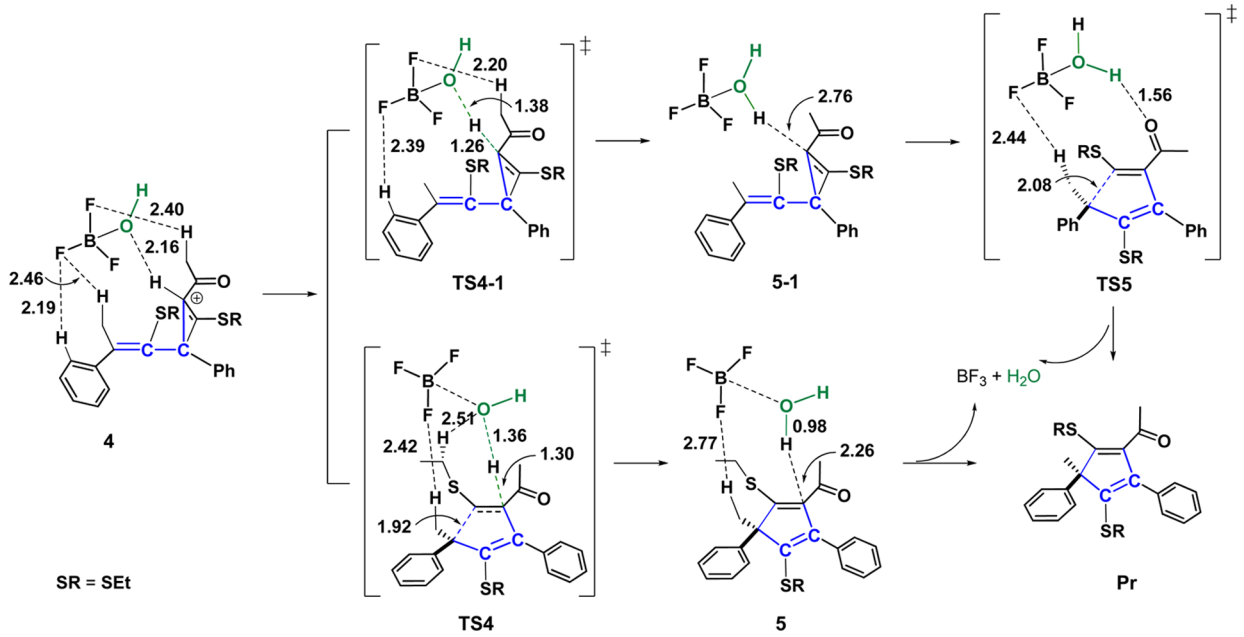


**Figure 4.** Structures in deprotonation and cyclization process of path A. Distances are in angstroms.

state **TS4−1** and five-membered ring transition state **TS5** (Figure 1, pink line). The $\Delta\Delta G^{\ddagger}$ value of **TS4−1** is 14.9 kcal/mol higher than that of **TS4**. Hence, path A is more favorable than path A3. Similarly for **4**, we examined three possible reaction pathways on **4-1**. Pathways A1, A1a, and A1b correspond to the concerted cyclization and alkylthio group shift (**4-1** → **4-2** → **TS4a1**), stepwise cyclization and alkylthio group shift (**4-1** → **TS4a** → **5a** → **TS5a**), as well as alkylthio group shift (**4-1** → **TS4b**) processes (Figure 5). The high activation energy barriers of **TS4a1** (45.9 kcal/mol), **TS4a** (50.8 kcal/mol), and **TS4b** (62 kcal/mol) show that these three pathways are kinetically unfeasible. Although path A1 is more favored than path A by 22.6 kcal/mol of $\Delta\Delta G^{\ddagger}$ for the $H^{\alpha}$-elimination, the higher barrier of the concerted cyclization and alkylthio group shift (**4-2** → **TS4a1**, $\Delta\Delta G^{\ddagger}$ = 45.9 kcal/mol) ruled out this path. Consequently, the comparison of the


DOI: 10.1021/acs.joc.5b02826
J. Org. Chem. 2016, 81, 1989−1997

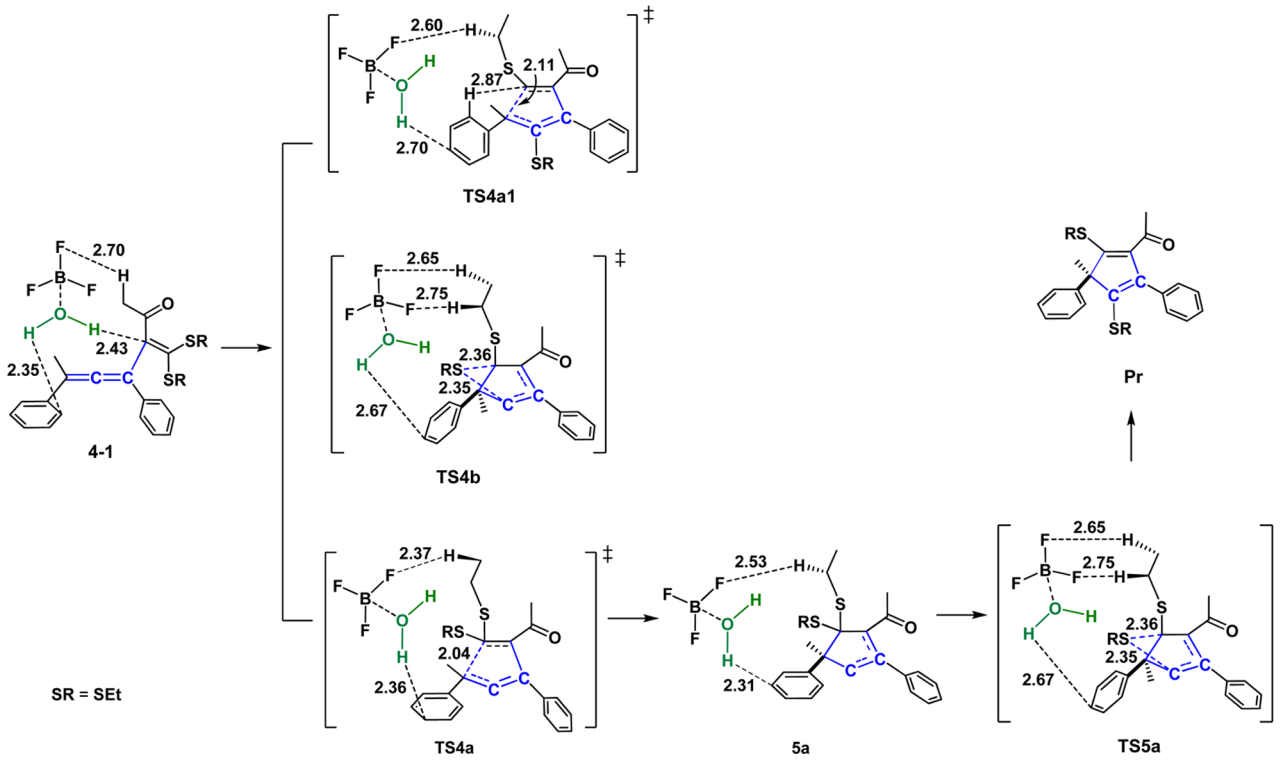


**Figure 5.** Structures in cyclization and alkylthio group shift of path A1. Distances are in angstroms.

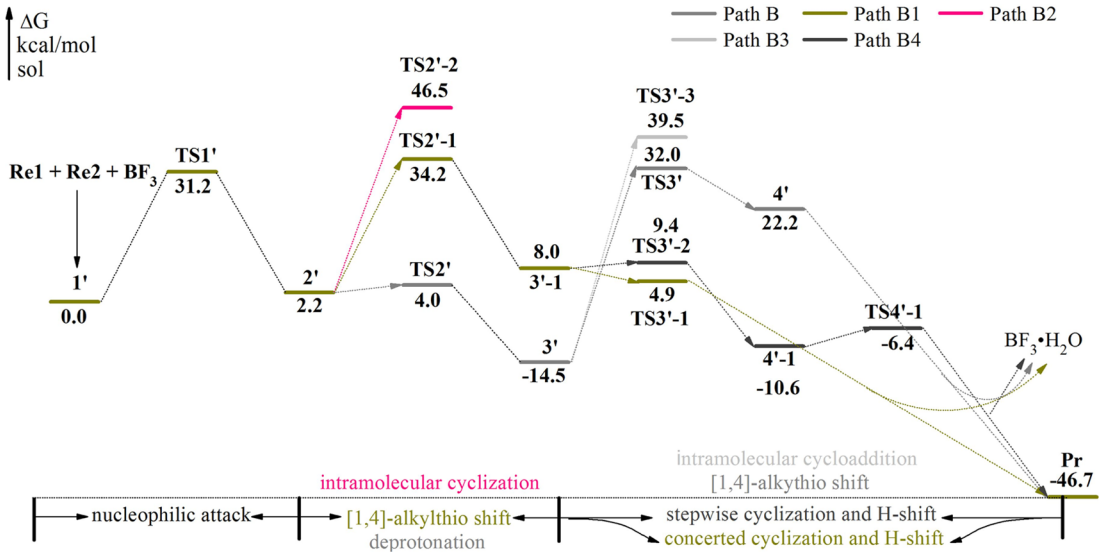


**Figure 6.** Energy profiles of the effect of different addition orientations of substrate **Re1** on the reaction mechanism. Values in kcal/mol are in the solvent phase.

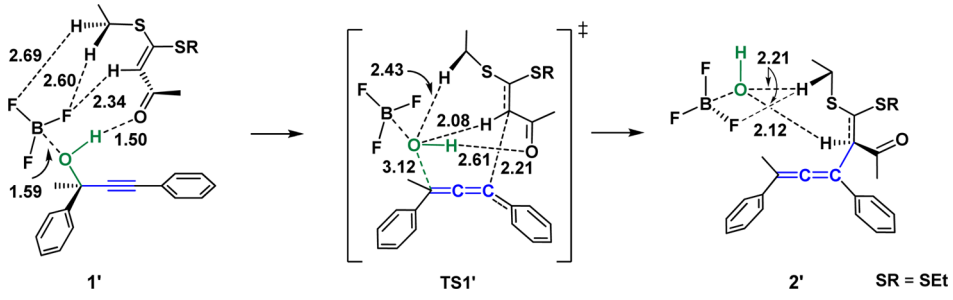


**Figure 7.** Structures of nucleophilic addition process in path B. Distances are in angstroms.



DOI: 10.1021/acs.joc.5b02826
J. Org. Chem. 2016, 81, 1989−1997

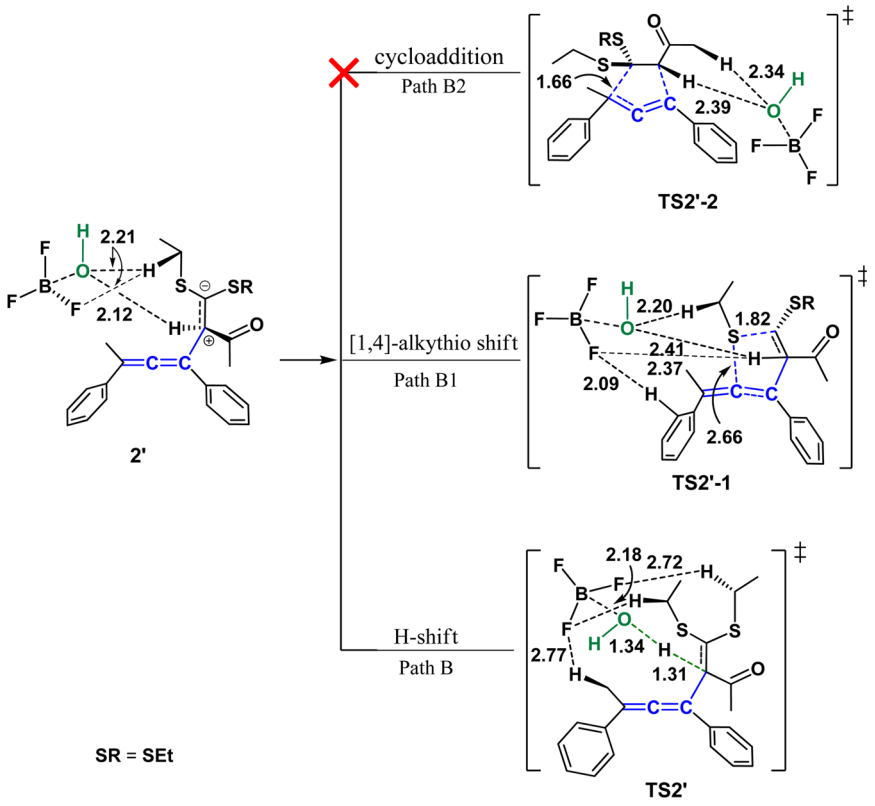


**Figure 8.** Comparison of the structures in [1,4]-alkylthio shift of path B1, H-shift of path B, and cycloaddition of path B2. Distances are in angstroms.

energy profiles (see Figure 1) for these five pathways conveys that the TS in path A is much more stable than path A1 by 12.7 kcal/mol. According to Figure 1, [1,4]-alkylthio shift (**3** → **TS3**, $\Delta G/\Delta\Delta G^{\ddagger}$ = 8.8/33.2 kcal/mol) is the rate-determining step of path A.

To investigate the effect of different addition orientation of substrate **Re1** on the reaction mechanism, we explored alternative possible pathway path B (Figure 6). It is worth noting that the differences between **2** and **1**′ lie in the opposite combinational direction of $\alpha$-oxo ketene dithioacetals to substrate **Re2** (Figures 2 and 7). Complex **1**′ initially undergoes the $BF_3$-catalyzed −OH elimination and nucleophilic attack of $C^{\alpha}$ of **Re1** on C3 of **Re2** via a concerted transition state **TS1**′ (31.2 kcal/mol) to form the zwitterionic intermediate **2**′. Subsequently, from **2**′, three distinct pathways were investigated (Figures 6 and 8). $H^{\alpha}$ deprotonation proceeded via **TS2**′ of 1.8 kcal/mol to form **3**′ (path B, gray line) or [1,4]-alkylthio shift (**TS2**′**-1**) to provide **3**′**-1** with an activation barrier of 32.0 kcal/mol (path B1, dark yellow line) as well as intramolecular cyclization via **TS2**′**-2** with the $\Delta\Delta G^{\ddagger}$ value of 44.3 kcal/mol (path B2, pink line). The computed activation barrier of the **TS2**′**-1** and **TS2**′ is 42.5 and 12.3 kcal/mol lower than that of **TS2**′**-2**. Similar to path A2, a preferential cyclization is a kinetically unfavorable process, which thus ruled out path B2. Afterward, path B included two competing processes, [1,4]-alkylthio shift (path B) and intramolecular cycloaddition (path B3). The high activation barriers of corresponding transition states **TS3**′ (46.5 kcal/mol) and **TS3**′**-3** (54.0 kcal/mol) in paths B and B3 exclude path B.

We consider two possible pathways in the processes of cyclization and H-shift from **3**′**-1** (Figure 9). Path B1 is the intramolecular cyclization between $C^{\beta}$ and C1 and $H^{\alpha}$ shifts from $C^{\alpha}$ to the −OH group via a concerted transition state **TS3**′**-1** (−3.1 kcal/mol). Path B4 is a stepwise process via five-membered ring and H-shift transition states **TS3**′**-2** (1.4 kcal/mol) and **TS4**′**-1** (4.2 kcal/mol) assisted by $[BF_3{\cdot}OH]^-$. The $\Delta\Delta G^{\ddagger}$ value of **TS4**′**-1** is higher than that of **TS3**′**-1** by 7.3 kcal/mol. Then the product **Pr** is formed by $BF_3$ and $H_2O$ releasing. As displayed in Figure 6, path B1 is the dominant reaction channel among the three pathways and the corresponding rate-determining step is [1,4]-alkylthio shift with the relative/activation free energy ($\Delta G/\Delta\Delta G^{\ddagger}$) barrier of 34.2/32.0 kcal/mol.

As shown in Figures 1 and 6, the rate-determining steps are predicted to be the [1,4]-alkylthio shift for paths A and B1, respectively. Although the $\Delta\Delta G^{\ddagger}$ value of **TS2**′**-1** is slightly lower than that of **TS3** by 1.2 kcal/mol, the $\Delta G$ value of **TS2**′**-1** is 25.4 kcal/mol higher than the latter one. Additionally, the addition orientation of the alkylthio group less affects the reaction mechanism and free activation energies except the H-shift and intramolecular cyclization processes. However, it exerts a pronounced effect on the potential energy surface, and a comparison of Figures 2 and 6 revealed that the relative energies of TSs in path A are much lower than those in path B1. Therefore, the computational results suggested that $BF_3$ $[BF_3{\cdot}OH]^-$ assisted path B1 is competitive with path A, and path A is relatively preferred kinetically. Furthermore, we also calculated single-point energies at the B3LYP-D/6-311+G** level (Figures S2 and S3). Our computational results indicated that B3LYP-D and M06-2X functionals give the same trend in the relative energies of transition states and intermediates. In addition, the relative energies of transition states and intermediates on the potential energy surfaces in paths A at the B3LYP-D/6-311+G** level are slightly lower than those at


DOI: 10.1021/acs.joc.5b02826
J. Org. Chem. 2016, 81, 1989−1997

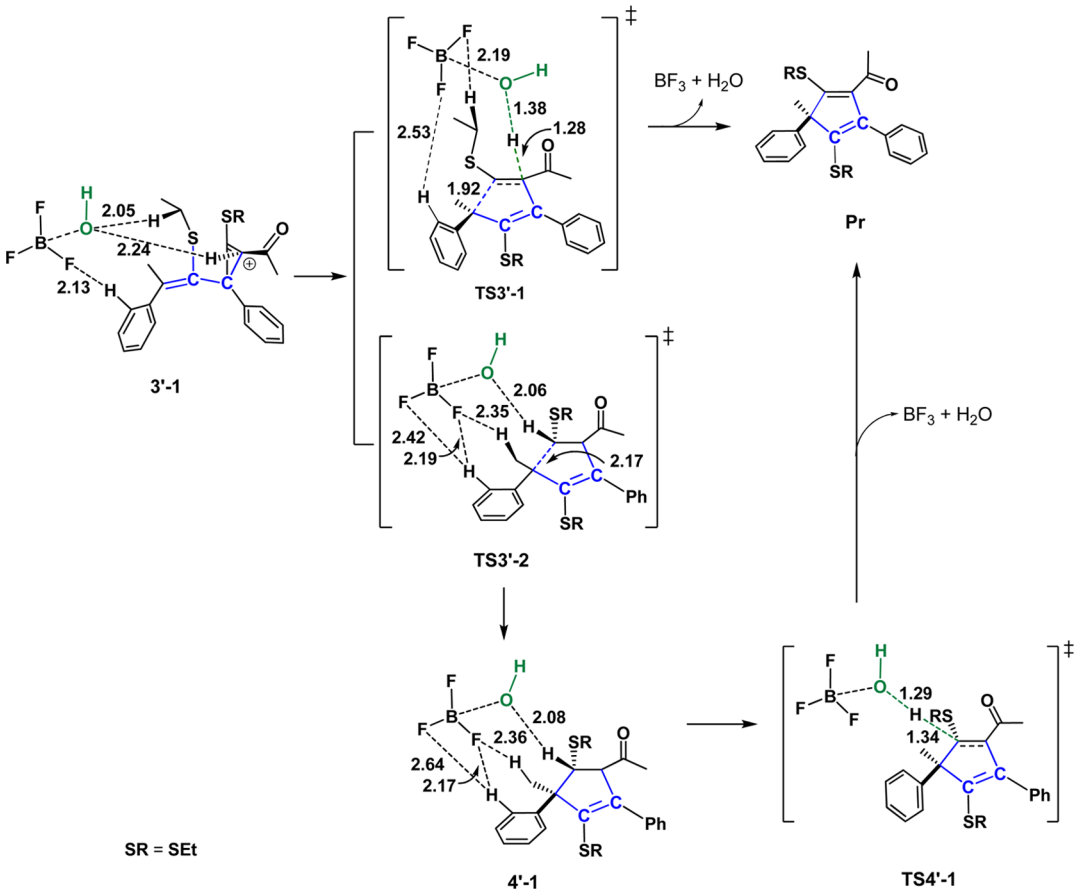


**Figure 9.** Structures in cyclization and H-shift process of path B1. Distances are in angstroms.

M06-2X/6-311+G** cases. However, the former activation energy barrier of [1,4]-alkylthio shift in the rate-determining step is 37.0 and 3.8 kcal/mol higher than the latter case. Thus, the computed results using M06-2X/6-311+G** functional are more reasonable and matched the experimental conditions ($T$ = 60 °C).

**3.3. NBO Analysis.** To further elucidate the origin of the difference of the orentation effect of alkylthio group on the reaction activity, we performed a second-order perturbation analysis on the two rate-determining step transition states **TS3** and **TS2′-1**. Second-order perturbation stabilization energies ($E(2)$) are the donor and acceptor interactions of the NBO Lewis bonding molecular orbitals to the antibonding molecular orbitals.[20b] As displayed in Table S1, the $E(2)$ values of n → n* and n → $\pi$* interactions of **TS3** between S1 and C2 as well as C1−C2 are 46.22 and 2.83 kcal/mol, respectively, which is larger than those in **TS2′-1** (37.72 and 1.53 kcal/mol). The results suggest that [1,4]-alkylthio shift catalyzed by $[BF_3{\cdot}OH]^-$ in path A is favored over that of path B1. It is consistent with the S1···C2 distance order of **TS3** (2.62 Å) < **TS2′-1** (2.66 Å). Moreover, the inspection of the structures of these two transition states shows the dihedral angle S1−$C^{\beta}$−C3−C2 in **TS3** is smaller than that in **TS2′-1** (3.8° vs −5.1°). Thus, $[BF_3{\cdot}OH]^-$ efficiently stabilizes the structure of **TS3** and reduces the relative free energy of the potential surface in the [1,4]-alkylthio shift step. The catalyst $[BF_3{\cdot}OH]^-$ plays an anchoring role by binding to the S atom of alkylthio group and the C1 atom of allenic carbon via multiple hydrogen bonds. Thus, the **TS3** is stabilized by strong double (O1···H1′−C1′, F1···$H^{\alpha}$−$C^{\alpha}$) and weak triple (F2···H4−C7, F1···H2−C8, F1···H3′−C3′) interactions with the total stabilization energy amount to 15.86 kcal/mol. Five kinds of hydrogen bonding interactions (O1···$H^{\alpha}$−$C^{\alpha}$, O1···H2′−C2′, O1···H3′−C3′, F1···H4−C7, F1···$H^{\alpha}$−$C^{\alpha}$) are found in the **TS2′-1**, and the sum of the $E(2)$ value is 11.81 kcal/mol. Consequently, the NBO calculation results further confirm that the $BF_3$ $[BF_3{\cdot}OH]^-$ catalyzed [3 + 2] cyclization path A is the more favored pathway relative to path B1. Similarly, the dispersion-corrected DFT methods B3LYP-D, PBE0-D, and M06 also show similar results (see Tables S2−S4). In addition, the higher activity of the [1,4]-alkylthio shift at **TS3** is also attributed to greater orbital overlap of the HOMO-8. As illustrated in Figure 10, the orbital interaction of the reaction site (C2···S1) in the case of **TS3** is larger than that in **TS2′-1** because the electron extensively delocalizes over the S1, C2−C3, $-CH_3$, and benzene ring part (pink ellipse). Therefore, the orbital analysis further identifies the rationalization of the calculation results mentioned above.

To unravel the noncovalent interactions of the active reaction site between S1 atom and allenic carbon (C2), we employed the Multiwfn[21] and VMD[25] to conduct electron densities and reduced density gradient RDG[26] isosurface for the rate-determining step structures. As shown in Figure 11, it is clear that the electrostatic interaction of the S atom and the C2 in **TS3** is stronger than that in **TS2′-1** represented by the deeper blue color (marked by purple square, in blue). Moreover, a strong stabilizing F···H−C hydrogen bond interaction is found in the transition state **TS3** (orange ellipse and arrow mark, in aquamarine blue), which is absent in the **TS2′-1**. Thus, the structure of **TS3** is much more stabilized by the noncovalent interactions as compared to **TS2′-1**.



DOI: 10.1021/acs.joc.5b02826
J. Org. Chem. 2016, 81, 1989−1997

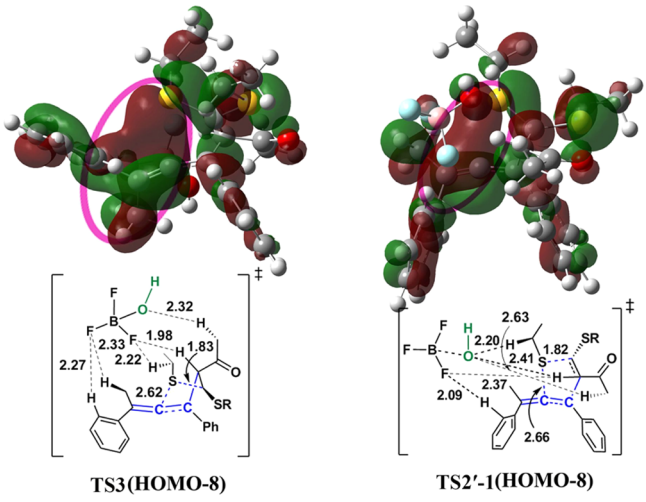


**Figure 10.** Orbital interactions in HOMOs of the $[BF_3{\cdot}OH]^-$ catalyzed transition states **TS3** and **TS2′-1**.

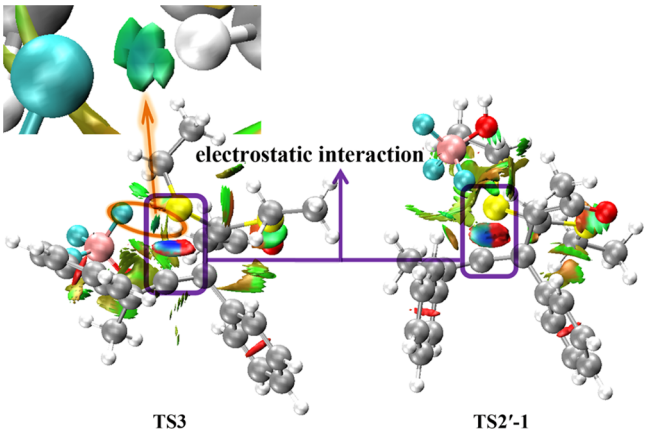


**Figure 11.** Noncovalent interactions analysis (blue, strong interaction; green, weak interaction; and red, strong repulsion) for $[BF_3{\cdot}OH]^-$ catalyzed alkylthio group shift transition states **TS3** and **TS2′-1**.

## CONCLUSION

We have carried out a mechanistic study to elucidate the mechanism of $BF_3$-catalyzed [3 + 2] cycloaddition between propargylic alcohol and $\alpha$-oxo ketene dithioacetals. The most favorable pathway for [1,4]-alkylthio shift prior to cyclization and H-elimination reaction labeled as path A consists of dehydroxylation, nucleophilic addition, [1,4]-alkylthio shift, and concerted deprotonation and cyclization. The calculated results suggest that electrophile $BF_3$ plays an important role to activate the reactive sites and efficiently stabilize the structures of transition states by multiple hydrogen bonding and electrostatic interaction. This is further confirmed by the NBO and noncovalent analyses. In addition, the investigation of different addition orientations of substrate **Re1** on the reaction mechanism suggests that it significantly affects the potential energy surface and reduces the relative energies of TSs in path A as compared to path B1. Therefore, our computational results indicated that the origin of different reactivity in paths A and B1 stems from the differences in F···H−C nonbonding interactions of the $BF_3$ $[BF_3{\cdot}OH]^-$ catalyzed the rate-determining step transition states.

## ASSOCIATED CONTENT

### Supporting Information

The Supporting Information is available free of charge on the ACS Publications website at DOI: 10.1021/acs.joc.5b02826.

Coordination modes of the catalyst $BF_3$ to the oxygen atoms of the substrates; Cartesian coordinates (PDF)

## AUTHOR INFORMATION

### Corresponding Author

*E-mail: jpzhang@nenu.edu.cn.

### Notes

The authors declare no competing financial interest.

## ACKNOWLEDGMENTS

Financial support by the National Natural Science Foundation of China (21173037, 21573036) is gratefully acknowledged.

## REFERENCES

(1) (a) Hartley, R. C.; Caldwell, S. T. J. *Chem. Soc., Perkin Trans. 1* **2000**, 477−501. (b) Wu, H.; Zhang, H.; Zhao, G. *Tetrahedron* **2007**, *63*, 6454−6461.

(2) (a) Williams, R. M.; Cox, R. J. *Acc. Chem. Res.* **2003**, *36*, 127−139. (b) Tsuda, M.; Kasai, Y.; Komatsu, K.; Sone, T.; Tanaka, M.; Mikami, Y.; Kobayashi, J. *Org. Lett.* **2004**, *6*, 3087−3089. (c) Martirosyan, A. O.; Gasparyan, S. P.; Aleksanyan, M. V.; Oganesyan, V. E.; Martirosyan, V. V.; Chachoyan, A. A.; Garibdzhanyan, B. T. *Pharm. Chem. J.* **2010**, *44*, 115−116.

(3) Zhang, X.-N.; Shi, M. *ACS Catal.* **2013**, *3*, 507−512.

(4) (a) Huisgen, R.; Bayer, H. O.; Schaefer, F. C.; Gotthardt, H. *Angew. Chem., Int. Ed. Engl.* **1964**, *3*, 136−137. (b) Huisgen, R.; Otto, P. *Tetrahedron Lett.* **1968**, *9*, 4491−4495. (c) Huisgen, R.; Brunn, E.; Gilardi, R.; Karle, I. *J. Am. Chem. Soc.* **1969**, *91*, 7766−7767. (d) Gothelf, K. V.; Jorgensen, K. A. *Chem. Rev.* **1998**, *98*, 863−909. (e) Bartok, M. *Chem. Rev.* **2010**, *110*, 1663−1705. (f) Xing, Y.; Wang, N.-X. *Coord. Chem. Rev.* **2012**, *256*, 938−952. (g) Tian, Z.; Xiao, Y.; Yuan, X.; Chen, Z.; Zhang, J.; Ma, J. *Organometallics* **2014**, *33*, 1715−1725.

(5) (a) Straus, D. S.; Glass, C. K. *Med. Res. Rev.* **2001**, *21*, 185−210. (b) Chang, H.-T.; Jayanth, T. T.; Cheng, C.-H. *J. Am. Chem. Soc.* **2007**, *129*, 4166−4167. (c) Jiao, L.; Lin, M.; Yu, Z.-X. *J. Am. Chem. Soc.* **2011**, *133*, 447−461.

(6) (a) Wang, Z.; Fang, H.; Xi, Z. *Tetrahedron* **2006**, *62*, 6967−6972. (b) Fang, H.; Li, G.; Mao, G.; Xi, Z. *Chem. - Eur. J.* **2004**, *10*, 3444−3450. (c) Chen, X.; Lu, P.; Wang, Y. *Chem. - Eur. J.* **2011**, *17*, 8105−8114. (d) Lee, J. H.; Toste, F. D. *Angew. Chem., Int. Ed.* **2007**, *46*, 912−914. (e) Funami, H.; Kusama, H.; Iwasawa, N. *Angew. Chem., Int. Ed.* **2007**, *46*, 909−911. (f) Sanjuán, A. M.; García-García, P.; Fernández-Rodríguez, M. A.; Sanz, R. *Adv. Synth. Catal.* **2013**, *355*, 1955−1962. (g) Shibata, Y.; Noguchi, K.; Tanaka, K. *J. Am. Chem. Soc.* **2010**, *132*, 7896−7898. (h) Rettenmeier, E.; Schuster, A. M.; Rudolph, M.; Rominger, F.; Gade, C. A.; Hashmi, A. S. K. *Angew. Chem., Int. Ed.* **2013**, *52*, 5880−5884. (i) Gao, Y.; Wu, W.; Huang, H.; Huang, Y.; Jiang, H. *Chem. Commun.* **2014**, *50*, 846−848.

(7) (a) Zhang, C.; Lu, X. *J. Org. Chem.* **1995**, *60*, 2906−2908. (b) Zheng, S.; Lu, X. *Org. Lett.* **2008**, *10*, 4481−4484. (c) Lu, Z.; Zheng, S.; Zhang, X.; Lu, X. *Org. Lett.* **2008**, *10*, 3267−3270.

(8) Fang, Z.; Liu, J.; Liu, Q.; Bi, X. *Angew. Chem., Int. Ed.* **2014**, *53*, 7209−7213.

(9) (a) Yuan, H.; Wang, M.; Liu, Y.; Wang, L.; Liu, J.; Liu, Q. *Chem. - Eur. J.* **2010**, *16*, 13450−13457. (b) Liang, D.; Wang, M.; Bekturhun, B.; Xiong, B.; Liu, Q. *Adv. Synth. Catal.* **2010**, *352*, 1593−1599. (c) Liu, Y.; Wang, M.; Yuan, H.; Liu, Q. *Adv. Synth. Catal.* **2010**, *352*, 884−892. (d) Yuan, H.-J.; Wang, M.; Liu, Y.-J.; Liu, Q. *Adv. Synth. Catal.* **2009**, *351*, 112−116. (e) Rao, H. S. P.; Sivakumar, S. *J. Org. Chem.* **2006**, *71*, 8715−8723.



DOI: 10.1021/acs.joc.5b02826
*J. Org. Chem.* 2016, 81, 1989−1997

(10) Frisch, M. J.; Trucks, G. W.; Schlegel, H. B.; Scuseria, G. E.; Robb, M. A.; Cheeseman, J. R.; Scalmani, G.; Barone, V.; Mennucci, B.; Petersson, G. A.; Nakatsuji, H.; Caricato, M.; Li, X.; Hratchian, H. P.; Izmaylov, A. F.; Bloino, J.; Zheng, G.; Sonnenberg, J. L.; Hada, M.; Ehara, M.; Toyota, K.; Fukuda, R.; Hasegawa, J.; Ishida, M.; Nakajima, T.; Honda, Y.; Kitao, O.; Nakai, H.; Vreven, T.; Montgomery, J. A., Jr.; Peralta, J. E.; Ogliaro, F.; Bearpark, M.; Heyd, J. J.; Brothers, E.; Kudin, K. N.; Staroverov, V. N.; Kobayashi, R.; Normand, J.; Raghavachari, K.; Rendell, A.; Burant, J. C.; Iyengar, S. S.; Tomasi, J.; Cossi, M.; Rega, N.; Millam, N. J.; Klene, M.; Knox, J. E.; Cross, J. B.; Bakken, V.; Adamo, C.; Jaramillo, J.; Gomperts, R.; Stratmann, R. E.; Yazyev, O.; Austin, A. J.; Cammi, R.; Pomelli, C.; Ochterski, J. W.; Martin, R. L.; Morokuma, K.; Zakrzewski, V. G.; Voth, G. A.; Salvador, P.; Dannenberg, J. J.; Dapprich, S.; Daniels, A. D.; Farkas, Ö.; Foresman, J. B.; Ortiz, J. V.; Cioslowski, J.; Fox, D. J. Gaussian 09; Gaussian, Inc.: Wallingford, CT, 2009.
(11) (a) Becke, A. D. *Phys. Rev. A: At., Mol., Opt. Phys.* **1988**, *38*, 3098−3100. (b) Lee, C.; Yang, W.; Parr, R. G. *Phys. Rev. B: Condens. Matter Mater. Phys.* **1988**, *37*, 785−789.
(12) (a) Gonzalez, C.; Schlegel, H. B. *J. Chem. Phys.* **1989**, *90*, 2154−2161. (b) Gonzalez, C.; Schlegel, H. B. *J. Phys. Chem.* **1990**, *94*, 5523−5527.
(13) Zhao, Y.; Truhlar, D. G. *Theor. Chem. Acc.* **2008**, *120*, 215−241.
(14) Koeller, S.; Thomas, C.; Peruch, F.; Deffieux, A.; Massip, S.; Léger, J.-M.; Desvergne, J.-P.; Milet, A.; Bibal, B. *Chem. - Eur. J.* **2014**, *20*, 2849−2859.
(15) Grimme, S. *J. Comput. Chem.* **2006**, *27*, 1787−1799.
(16) Krenske, E. H.; Davison, E. C.; Forbes, I. T.; Warner, J. A.; Smith, A. L.; Holmes, A. B.; Houk, K. N. *J. Am. Chem. Soc.* **2012**, *134*, 2434−2441.
(17) (a) Yang, H.; Wong, M. W. *J. Am. Chem. Soc.* **2013**, *135*, 5808−5818. (b) Cho, B.; Tan, C. H.; Wong, M. W. *Org. Biomol. Chem.* **2011**, *9*, 4550−4557. (c) Yang, H.; Wong, M. W. *J. Org. Chem.* **2011**, *76*, 7399−7405. (d) Wong, M. W.; Ng, A. M. E. *Aust. J. Chem.* **2014**, *67*, 1100−1109. (e) Zhao, Y.; Truhlar, D. G. *Acc. Chem. Res.* **2008**, *41*, 157−167. (f) Xue, H.; Jiang, D.; Jiang, H.; Kee, C. W.; Hirao, H.; Nishimura, T.; Wong, M. W.; Tan, C. H. *J. Org. Chem.* **2015**, *80*, 5745−5752.
(18) (a) Marenich, A. V.; Cramer, C. J.; Truhlar, D. G. *J. Phys. Chem. B* **2009**, *113*, 6378−6396. (b) Yang, Y. F.; Cheng, G. J.; Liu, P.; Leow, D.; Sun, T. Y.; Chen, P.; Zhang, X. H.; Yu, J. Q.; Wu, Y. D.; Houk, K. N. *J. Am. Chem. Soc.* **2014**, *136*, 344−355.
(19) (a) Zhao, Y.; Truhlar, D. G. *Chem. Phys. Lett.* **2011**, *502*, 1−13. (b) Vrcek, V.; Mestric, H. *J. Phys. Org. Chem.* **2009**, *22*, 59−68. (c) Wakamatsu, K.; Orita, A.; Otera, J. *Organometallics* **2010**, *29*, 1290−1295. (d) Voukides, A. C.; Konrad, K. M.; Johnson, R. P. *J. Org. Chem.* **2009**, *74*, 2108−2113.
(20) (a) Reed, A. E.; Curtiss, L. A.; Weinhold, F. *Chem. Rev.* **1988**, *88*, 899−926. (b) Cho, B.; Tan, C.-H.; Wong, M. W. *J. Org. Chem.* **2012**, *77*, 6553−6562. (c) Yang, H.; Wong, M. W. *Org. Biomol. Chem.* **2012**, *10*, 3229−3235.
(21) (a) Bader, R. F. W. *Atoms in Molecules: A Quantum Theory*; Clarendon Press: Oxford, 1990. (b) Lu, T.; Chen, F. W. *J. Comput. Chem.* **2012**, *33*, 580−592. (c) Jindal, G.; Sunoj, R. B. *Angew. Chem., Int. Ed.* **2014**, *53*, 4432−4436. (d) Reddi, Y.; Sunoj, R. B. *ACS Catal.* **2015**, *5*, 5794−5802. (e) Reddi, Y.; Sunoj, R. B. *ACS Catal.* **2015**, *5*, 1596−1603.
(22) Legault, C. Y. *CYLView, 1.0b*; Université de Sherbrooke: Canada, 2009; http://www.cylview.org.
(23) (a) Méndez, P. S.; Cachau, R. E.; Seoane, G.; Ventura, O. N. *J. Mol. Struct.: THEOCHEM* **2009**, *904*, 21−27. (b) Jaric, M.; Haag, B. A.; Unsinn, A.; Karaghiosoff, K.; Knochel, P. *Angew. Chem., Int. Ed.* **2010**, *49*, 5451−5455. (c) Kessar, S. V.; Singh, P.; Singh, K. N.; Bharatam, P. V.; Sharma, A. K.; Lata, S.; Kaur, A. *Angew. Chem., Int. Ed.* **2008**, *47*, 4703−4706.
(24) Zhu, Y.; Sun, L.; Lu, P.; Wang, Y. *ACS Catal.* **2014**, *4*, 1911−1925.
(25) Humphrey, W.; Dalke, A.; Schulten, K. *J. Mol. Graphics* **1996**, *14*, 33−38.
(26) (a) Johnson, E. R.; Keinan, S.; Mori-Sánchez, P.; Contreras-García, J.; Cohen, A. J.; Yang, W. T. *J. Am. Chem. Soc.* **2010**, *132*, 6498−6506. (b) Xue, X. S.; Li, X.; Yu, A.; Yang, C.; Song, C.; Cheng, J. P. *J. Am. Chem. Soc.* **2013**, *135*, 7462−7473. (c) Contreras-García, J.; Johnson, E. R.; Keinan, S.; Chaudret, R.; Piquemal, J. P.; Beratan, D. N.; Yang, W. T. *J. Chem. Theory Comput.* **2011**, *7*, 625−632.


DOI: 10.1021/acs.joc.5b02826
*J. Org. Chem.* 2016, 81, 1989−1997